SLAC-PUB-12489

LINAC COHERENT LIGHT SOURCE ELECTRON BEAM COLLIMATION*

P. Emma, D. Dowell, C. Limborg, J. Schmerge, J. Wu, SLAC, Menlo Park, CA 94025, USA

Abstract

This paper describes the design and simulation of the electron beam collimation system in the Linac Coherent Light Source (LCLS). Dark current is expected from the gun and some of the accelerating cavities. Particle tracking of the expected dark current through the entire LCLS linac, from gun through FEL undulator, is used to estimate final particle extent in the undulator as well as expected beam loss at each collimator or aperture restriction. A table of collimators and aperture restrictions is listed along with halo particle loss results, which includes an estimate of average continuous beam power lost. In addition, the transverse wakefield alignment tolerances are calculated for each collimator.

Halo Particle (Dark Current) Tracking

Electron beam collimation is necessary in the LCLS [1] in order to remove halo particles in the linac, before they impact and eventually degrade the very precise fields of the permanent magnet undulator. In order to do a simple test of the effectiveness of the LCLS linac collimation system, particle tracking is done through the entire linac with halo particles in all six phase space dimensions. The halo is generated from the spatial and temporal extent of the electron gun-generated dark current emission from the cathode. Besides this, there are also a few accelerator cavities which will generate dark current, adding to the halo particles. The largest amplitude particles remaining after acceleration and collimation are found to be smaller than the undulator aperture. In addition, a rough estimate is made of the average continuous beam power lost on each individual collimator under nominal operating conditions, and assuming a worst case dark current scenario, which consists of a bunch repetition rate of 120 Hz, 3 nC of dark current generated at the cathode over a 1-μs RF pulse length at $E_{\rm RF} = 120$ MV/m, and 15 pC over a 2-μs wide macro pulse in each single 3-m SLAC structure at $E_{\rm RF} = 26$ MV/m.

The dark current is generated in the code *Parmela* [2], following the Fowler-Nordheim model, which reads [3]

$$I_{\rm FN} = 1.54 \times 10^{-6} \frac{\beta_e^2 A_e E_{\rm RF}^2}{\varphi} 10^{4.52\varphi^{-0.5}} e^{-\frac{6.53\times 10^9 \varphi^{1.5}}{\beta_e E_{\rm RF}}}, \quad (1)$$

where $I_{\rm FN}$ is the dark current in units of A, β_e the field enhancement factor, φ the work function of the metal in eV (for copper, $\varphi = 4.7$ eV), A_e the effective emission area in m^2, and $E_{\rm RF}$ the applied electric field in V/m. In the simulation, the time varying electric field $E_{\rm RF}$ on the cathode is used to calculate the number of particles emitted over the accelerating half of the RF period. The transverse distribution on the cathode is taken as a uniform cylinder with a radius of 2.5 mm, which is sufficient, since almost all particles with larger radius than 2.5 mm are lost in the injector. In the simulation, 4×10^5 macro particles are used at the cathode to represent the charge in one RF bucket.

According to the *Parmela* simulation, there are 3.4×10^5 macro particles at the end of the gun, out of the initial 4×10^5 macro particles at the cathode for a spot of $r = 2.5$ mm. Based on experiment at the end of gun, there are up to 3 nC dark current over a 1-μs wide macro pulse (~ 3000 RF buckets) at $E_{\rm RF} = 120$ MV/m. Hence, we use this 3.4×10^5 macro particles to represent the charge in one bucket of this 3-nC of dark current, and also use this to normalize the dark current from the 3-m RF structure.

For an s-band RF structure we have one experimental data point, *i.e.*, about 15 pC over a 2-μs wide macro pulse in a single 3-m SLAC structure at $E_{\rm RF} = 26$ MV/m. Hence, we use 850 macro particles to simulate the charge in one bucket of this 15-pC of structure current. This 15-pC represents 7.5 μA of captured dark current observed in experiment. According to simulation, this 15-pC is only 10% of the generated charge ($I_{\rm FN} = 75$ μA). We take a realistic set of $\beta_e = 120$, $A_e = 350$ μm^2 in Eq. (1) and the same 10% capture rate for $E_{\rm RF} = 24$ MV/m, and use about 120 macro particles per bucket to represent this captured structure current. While at $E_{\rm RF} = 20$ MV/m, the number drops to 1 macro particle per bucket. We then use the corresponding number of macro particles for each s-band RF cavity according to its accelerating gradient along the LCLS accelerator system. For the x-band RF cavity, we have $\beta_e \approx 30$, and $E_{\rm RF} = 31.7$ MV/m, hence there is essentially no dark current generated.

The dark current generated from the cathode is accelerated using *Parmela* to the end of the first 3-m long accelerating section where the design energy is nominally 64 MeV. The velocity slippage is included in the *Parmela* propagation such that the RF phase is not constant, leading to only a very few macro particles (2×10^4 or 5%) transmitted to the nominal 64-MeV point. In addition, a second delayed RF bucket is seen to form. These delayed particles are manually forced into the main RF bucket by shifting their phases forward 360°. This manipulation replicates the fact that the single bucket under study will be preceded by an earlier bucket with its own delayed particles.

From the 64-MeV point, the 2×10^4 macro particles are tracked through the nominal LCLS design using *elegant* [4] with canonical elements through the undulator. With the number of macro particles reduced from 3.4×10^5 to only 2×10^4 (0.06 pC per bucket) after the injector, wakefield and CSR effects in the linac are not important and are there-

* Work supported by the U.S. Department of Energy under Contract No. DE-AC02-76SF00515.

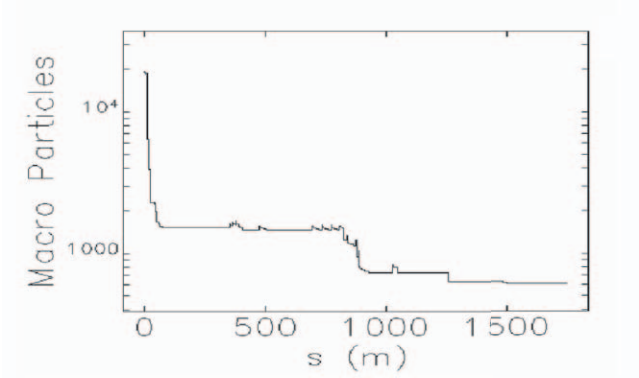

Figure 1: Beam transmission along LCLS linac with 2×10^4 macro particles remaining after the injector.

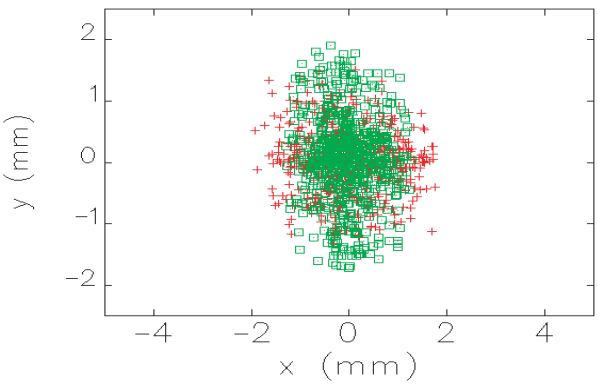

Figure 2: Scatter plot of x and y positions of all 614 remaining macro particles/bucket at $s = 64$ m (red +) and $s = 43$ m (green square) along the undulator. The plot boundaries represent the vacuum chamber walls.

fore switched off. In this simple model, the macro particle is completely lost when its position exceeds the aperture limit, with no edge scattering effects included. With the primary collimators 650 m up-beam of the undulator, this is not an unreasonable treatment.

As explained above, to protect the undulator, various collimation components (described in Table 1) are introduced along the LCLS accelerator system. The number of surviving macro particles along the accelerator is shown in Fig. 1. All but 614 macro particles/bucket (5 pC in the 1-μs macro pulse) are lost prior to the undulator. The transverse coordinates of these 614 macro particles are shown in Fig. 2 at two undulator locations, each at the worst case in one plane. No particle position exceeds the vacuum chamber walls (plot boundaries). Table 1 lists the various aperture restrictions used in the tracking and the particle loss results. Each aperture is listed with its name; linac location area; whether the aperture is fixed (f) or adjustable (a); whether the aperture limit is horizontal (x), vertical (y), cylindrical radius (r), or energy related (E is always horizontal); the distance (s) measured from the cathode along the linac axis to the aperture limit; the nominal beam energy (E); the nominal rms beam size ($\sigma_{x,y}$, assuming $\gamma\epsilon_{x,y} = 1.2$ μm); the aperture's half-width (a); the aperture's half-width in units of rms beam size ($a/\sigma_{x,y}$); the total charge lost at that point; the estimated average continuous beam power lost at that point at 120-Hz assuming 3 nC of total dark charge over the 1-μs RF pulse at the exit of the gun; and the transverse alignment tolerance for each collimator (see wakefield discussion below). In Table 1, several aperture limits are included to model the S-band iris (11.6 mm) and various 1-inch beam pipes.

Collimators

Adjustable beam collimation is accomplished in two main sections. The first (primary collimation) is the existing collimation section at the end of the SLAC linac, originally installed for SLC operations. This is composed of four horizontal and four vertical pairs of rectangular collimator jaws (CY29096 through CX30546 in Table 1), each independently and remotely adjustable in gap and center. The jaws are a Titanium alloy (Ti-6Al-4V) body with slightly curved face (10-m radius) and Titanium-Nitride jaw surface for improved conductivity and survivability against beam hits [5]. The second section (secondary collimation) is installed in the new transport beamline from linac to undulator (LTU, shown in Fig. 3). This is composed of three horizontal and thee vertical pairs of rectangular collimator jaws (CX31 through CY38 in Table 1). These are identical in design to those in the linac. Each collimator (per plane) is separated by about 90-degrees of betatron phase advance so that the first jaws collimate position, the second collimate angle, and the third perform a clean-up pass on edge scattering produced by the second. In addition there are two horizontal pairs of jaws (CEDL1 through CEDL3 in Table 1) in the preceding bending section which collimate off-energy particles where the absolute value of the momentum dispersion is 120 mm. Note it is not necessary to taper these jaws to limit wakefield effects, as is proposed in linear colliders [6]. The very short bunch and much larger emittance in an FEL accelerator make wakefield issues much less severe. Besides these two main sections, energy collimators are introduced inside both bunch compressors (CE11 for BC1, and CE21 for BC2). A section view of CE11 is shown in Fig. 4.

Collimator Wakefields

The emittance growth of the high-brightness electron-beam (with Gaussian longitudinal distribution) due to the transverse wakefield of a misaligned collimator with half-gap a in a beam pipe of radius $b \gg a$, and for our case, where the bunch length $\sigma_z \ll a$, is given by [7]

$$\frac{\epsilon}{\epsilon_0} \approx \sqrt{1 + \frac{4N^2 r_e^2 \beta}{3\gamma\epsilon_N}\left(\frac{1}{a^2} - \frac{1}{b^2}\right)^2 \Delta x^2}, \qquad (2)$$

where N is the number of electrons in the bunch (6.25×10^9), r_e is the classical electron radius, β is the beta-

Table 1: Halo propagation through the linac beam collimators and apertures. The text describes the data in detail.

aperture	**linac area**	**fixed/ adjust.**	x, y, r or E	s (m)	E (GeV)	σ_x **or** σ_y (mm)	a (mm)	$a/\sigma_{x,y}$	**loss** (pC)	**power** (W)	$\lvert\Delta x_{tol}\rvert$ (mm)
L0-iris	L0	f	r	5.3	0.064	0.56	$\pm$11.6	$\pm$21	2.0	0.02	-
L0-iris	L0	f	r	8.0	0.126	0.32	$\pm$11.6	$\pm$36	2.8	0.04	-
1" pipe	DL1	f	r	17.0	0.135	0.34	$\pm$12.7	$\pm$38	110	1.8	-
L1-iris	L1	f	r	20.3	0.135	0.21	$\pm$11.6	$\pm$55	14.6	0.2	-
L1-iris	L1	f	r	23.4	0.189	0.21	$\pm$11.6	$\pm$55	8.0	0.2	-
X-band	L1	f	r	29.8	0.268	0.16	$\pm$3.50	$\pm$22	14.3	0.5	-
CE11	BC1	a	E	34.6	0.250	3.7	$\pm$45.0	$\pm$12	0	0	1.0
L2-iris	L2	f	r	50.0	0.350	0.20	$\pm$11.6	$\pm$45	6.7	0.3	-
CE21	BC2	a	E	410.3	4.300	2.6	$\pm$36.0	$\pm$14	0.4	0.2	1.0
CY29096	sec-29	a	y	827.8	10.601	0.061	$\pm$1.60	$\pm$26	2.0	2.6	0.5
CX29146	sec-29	a	x	842.1	10.773	0.055	$\pm$1.60	$\pm$29	0.9	1.2	0.6
CY29446	sec-29	a	y	879.1	11.348	0.058	$\pm$1.60	$\pm$27	2.1	2.9	0.5
CX29546	sec-29	a	x	891.4	11.520	0.053	$\pm$1.60	$\pm$30	1.4	1.9	0.6
CY30096	sec-30	a	y	930.5	12.121	0.056	$\pm$1.80	$\pm$32	0.1	0.2	0.7
CX30146	sec-30	a	x	943.6	12.308	0.052	$\pm$1.80	$\pm$35	0.01	0.01	0.8
CY30446	sec-30	a	y	980.6	12.884	0.054	$\pm$1.80	$\pm$33	0	0	0.7
CX30546	sec-30	a	x	993.0	13.071	0.050	$\pm$1.80	$\pm$36	0	0	0.8
CEDL1	DL2	a	E	1257.0	13.640	0.12	$\pm$2.50	$\pm$21	0.8	1.4	0.5
CEDL3	DL2	a	E	1328.7	13.640	0.12	$\pm$2.50	$\pm$21	0.04	0.07	0.5
CX31	LTU	a	x	1419.1	13.640	0.055	$\pm$2.20	$\pm$40	0	0	1.0
CY32	LTU	a	y	1436.8	13.640	0.055	$\pm$2.20	$\pm$40	0	0	1.0
CX35	LTU	a	x	1489.7	13.640	0.055	$\pm$2.20	$\pm$40	0.1	0.2	1.0
CY36	LTU	a	y	1507.3	13.640	0.055	$\pm$2.20	$\pm$40	0.03	0.04	1.0
CX37	LTU	a	x	1520.5	13.640	0.051	$\pm$2.30	$\pm$45	0	0	1.0
CY38	LTU	a	y	1527.2	13.640	0.067	$\pm$3.20	$\pm$48	0	0	1.0
PCMUON	LTU	f	r	1547.7	13.640	0.040	$\pm$2.83	$\pm$71	0	0	1.0

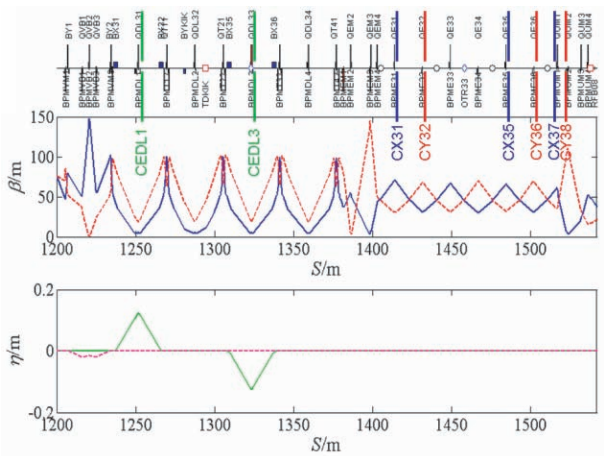

Figure 3: Collimation section in LTU with energy collimators in green, x-collimators in blue, and y in red. The undulator starts at the far right side of the plot.

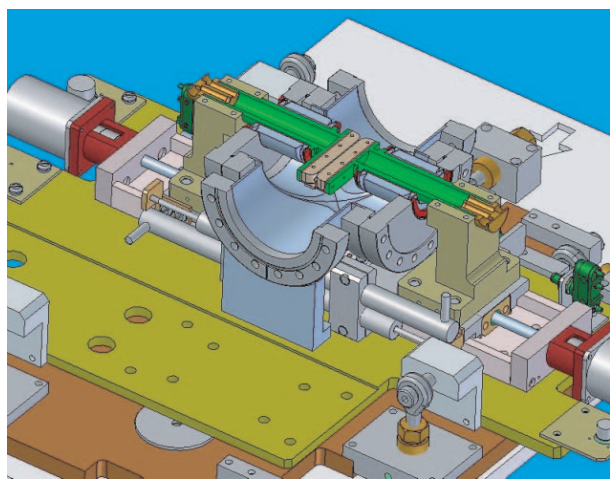

Figure 4: Section view of CE11 with jaws inserted.

function at the collimator, γ is the beam energy in rest mass units, ϵ_N is the normalized transverse emittance, and Δx is the transverse misalignment of the collimator gap. Table 1 lists the transverse alignment tolerances for each collimator in order to produce an emittance growth of $< 2\%$ each. (The tolerances here have been limited to ≤ 1 mm). The misalignment is in the plane of collimator gap, x, y, or r as listed in column 4 of the table. Longitudinal wakefields can also be important, especially at collimators with nonzero momentum dispersion (all E-collimators). None of the collimators listed here, however, will increase the emittance through the longitudinal wakefield by more than 1%.

REFERENCES

[1] *LCLS CDR*, SLAC Report No. SLAC-R-593, 2002.

[2] J. Billen, *PARMELA*, Los Alamos National Laboratory Report LA-UR-96-1835 (1996).

[3] J. Wang, Ph.D. thesis, SLAC Report No. SLC-R-339, 1989.

[4] M. Borland, APS LS-287, Sep. 2000.

[5] F.-J. Decker *et al.*, LINAC-96, p. 137, Geneva, Switz., 1996.

[6] P. Tenenbaum *et al.*, PAC-01, p. 418, Chicago, IL, 2001.

[7] F. Zimmermann *et al.*, EPAC-96, p. 540, Sitges, Spain, 1996.